

Blood-based hybrid nanofluid flow through converging/diverging channel with multiple slips effect: a development of Jeffery-Hamel problem

Saeed Dinarvand

*Department of Mechanical Engineering, Central Tehran Branch,
Islamic Azad University, Tehran, Iran*

Hamza Berrehal

*Department of Physics, Exact Science Faculty, Constantine 1 University,
Constantine, Algeria*

Ioan Pop

Department of Mathematics, Babes-Bolyai University, Cluj-Napoca, Romania, and

Ali. J. Chamkha

*Faculty of Engineering, Kuwait College of Science and Technology,
Doha District, Kuwait*

Abstract

Purpose – The purpose of this paper is to study and analyze the converging/diverging channel flow and heat transfer with the multiple slips effect, which is a development of the Jeffery–Hamel problem using the mass-based hybrid nanofluid algorithm. Whereas transferring biological liquid by arteries is a vital issue, mathematical modeling of hybrid nanofluid flow containing titanium dioxide and silver as nanoparticles and blood as base liquid through a converging/diverging duct, which can be a useful analysis for the fields of drug delivery, has been investigated.

Design/methodology/approach – The present approach is based on the Tiwari–Das nanofluid method. In this modeling, the volume fraction of nanoparticles is replaced with nanoparticles masses. The partial differential equations of the mass, momentum and energy conservations are changed to the system of ordinary differential equations through the similarity solution method. The final governing equations are solved by Runge–Kutta–Fehlberg procedure and shooting method.

Findings – The effect of emerging parameters on the temperature, the velocity, the Nusselt number and the skin friction have been analyzed by graphical and tabular reports. It is observed that the opposition to hybrid nanofluid flow in the attendance of particles of nonspherical shapes is more enhanced than those in the attendance of particles of spherical shapes. This issue demonstrates that the rheology of a hybrid nanofluid is dependent on the shape of particles. Besides, backflow regimes form in the divergent channel for high values of Reynolds number, m_2 and a . Indeed, this modeling for the hybrid nanofluid can be useful in different technologies and industries such as biological ones. It is worth mentioning that the excellent achievement of the mass-based algorithm for heat transfer and hybrid nanofluid flow is the most important success of this study.

Originality/value – The main originality is related to the development of the Jeffery–Hamel problem using the mass-based hybrid nanofluid algorithm. This new mass-based method is a single-phase hybrid nanofluid approach that the inputs are masses of nanoparticles and base liquid.



Besides, considering the multiple slips effect and also pure blood as base fluid in this problem are also new.

Keywords Converging/diverging channel, Blood flow, Hybrid nanofluid, Mass-based algorithm, Numerical method

Paper type Research paper

1. Introduction

As we know, nanotechnology is one of the most promising achievements of the 21st century. Indeed, it is the ability to change the nanoscience theory to beneficial applications by manipulating, assembling, measuring, observing, controlling as well as manufacturing material at the nanometer scale. Now, the evolution of nanoscience and nanotechnology is expected to bring multidimensional and unimaginable improvements to human life. In pioneer thermal engineering, outcomes of many experimental and theoretical studies are manifesting the amplification of thermal conductivity because of the suspension of nanoparticles in common heat transfer working fluids (Menni *et al.*, 2020; Sreedevi *et al.*, 2020). Nanoparticles (particles in dimensions of 1–100 nm) are composed of metals, oxides, carbon nanotubes and carbides. Water, oil, ethylene and many others are usually taken as base fluids. Indeed, the nanofluids include the mixture of base liquids and nanoparticles with a homogenous form. The shape and size of such nanoparticles accredit the heat transfer assessment of nanofluids (Jaballah *et al.*, 2019). The fluid with suspension of nanoparticles is analyzed in many applications such as nuclear sciences, plasma physics, energy enhancement, cooling and heating phenomenon and fission and fusion processes. Hybrid nanofluids are the mixture of two different particles of nonmetals or metals in working fluids with heat transfer applications (Afshari *et al.*, 2021; Agrawal *et al.*, 2021). More suitable thermophysical properties of new heat transfer fluids such as dynamic viscosity, thermal conductivity and density can be obtained by choosing the proper nanoparticles and base liquids (Waini *et al.*, 2021; Khan *et al.*, 2021; Waini *et al.*, 2020). Drug delivery, biomedical applications, solar energy applications, acoustics, transportation, micro-electrical, microfluid, manufacturing, propulsive, improved heat exchangers and many others, are some fields of hybrid nanofluids usage (Suresh *et al.*, 2011; Mahian *et al.*, 2021; Sibanda *et al.*, 2012; Berrehal *et al.*, 2022). In Table 1, a summary of characteristics for mono nanofluid and hybrid nanofluid has been presented that easily one can compare these two kinds of the working fluid.

Incompressible viscous fluid flow by a diverging/converging duct is generally known as Jeffery–Hamel flow (Ahmed *et al.*, 2018). This problem is a principal type of flow in the fluid mechanics field. Applications of the Jeffery–Hamel flow contains flow through rivers, various engineering processes as well as in the field of biology (Patel and Meher, 2018). Many scientists have made contributions considering the usages of Jeffery–Hamel flow during the recent years (Patel and Meher, 2018; Berrehal and Makinde, 2021).

Fraction-based analysis of nanofluids and hybrid nanofluids were paid attention by many researches, but Dinarvand (Dinarvand and Rostami, 2019; Dinarvand *et al.*, 2019) was the first who introduced the mass-based model. This new mass-based method is a single-phase hybrid nanofluid approach that the inputs are masses of nanoparticles and base liquid. Thus, with this introduction, the aim of this study is to identify and analyze the converging/diverging channel flow with multiple slips effect that is a development of Jeffery–Hamel problem using mass-based hybrid nanofluid algorithm. The governing ODEs are numerically analyzed and the results of the problem are shown for different emerging parameters. This approach suggests the new explanation for the thermophysical properties of hybrid nanofluid based on both nanoparticles and base liquid properties.

Key parameters	Single (or) mono nanofluid	Hybrid (or) nanocomposite nanofluid
<i>Preparation</i>	<ul style="list-style-type: none"> One-step and two-step methods have been followed by many researchers for the preparation of single nanofluid. Among the two methods, the two-step technique works well for oxide nanoparticles, while it is less successful, compared to single-step method, for metal nanoparticles Single nanoparticle is available commercial in many cases Size and shape of single nanoparticle can be controlled as required 	<ul style="list-style-type: none"> Two-step method has been employed by most researchers. The following points should be considered, before preparing hybrid nanofluids: choice of appropriate nanoparticles combination, synthesis of the nanocomposite particles, bonding between the nanoparticles involved in the composite and use of surfactant Composite nanoparticles are synthesized as they are not readily available Size and shape of composite nanoparticles cannot be controlled. In nanocomposite, two nanoparticles may overlap, arranged one by one (or) one particle is coated over other
<i>Properties (Thermal conductivity, Viscosity, Density)</i>	<ul style="list-style-type: none"> Single nanofluid have shown better enhancement in properties than base fluid In internal flow, enhancement of viscosity results in high pressure drop which increases the pumping power as compared to that of the base fluid Theoretical models are available in large numbers for thermophysical properties 	<ul style="list-style-type: none"> Hybrid nanofluid have shown still better enhancement in properties than single nanofluid In internal flow, enhancement of viscosity results in high pressure drop which slightly increases the pumping power than single nanofluid Limited theoretical models only are available for hybrid nanofluids
<i>Applications</i>	<ul style="list-style-type: none"> Single nanofluids are used in a variety of thermal energy exchange systems such as transportation, electronic cooling, energy storage and mechanical applications 	<ul style="list-style-type: none"> Very few applications such as heat sink, boiling heat transfer, heat exchanger, solar absorption, micro power generation and heat pipe are reported in literatures. However, hybrid nanofluids can be used in all applications wherever single nanofluids are used
<i>Stability</i>	<ul style="list-style-type: none"> Stability can be controlled with the use of surfactant In single nanofluids, stability can be maintained for long period 	<ul style="list-style-type: none"> In nanocomposite-based nanofluids, the dispersion of two different materials in composite form in the base fluid poses a considerable problem because of the surface charge (positive or negative), which varies from one-particle to another one

Table 1. Features of single and hybrid nanofluid in a glance (Jana *et al.*, 2007; Li *et al.*, 2021; Sidik *et al.*, 2017; Das, 2017; Ahmed *et al.*, 2021)

(continued)

Key

parameters

Single (or) mono nanofluid

Hybrid (or) nanocomposite nanofluid

- In hybrid nanofluids, the stability is complicated because of dispersion of two different nanoparticles in a base fluid, but nanocomposite particles possess extreme stability in a variety of aqueous solvents without any surfactant

Cost

- Cost of the nanofluid differs based on the type of nanoparticle selected. Metallic nanoparticle and Carbon nanotubes are much costlier than metal oxide nanoparticles
- A composite of only a small amount of metallic nanoparticle and oxide nanoparticle shows performance increment as good as single metallic nanofluid. But, cost of composite nanofluid is slightly less than metallic nanoparticle based single nanofluid

Table 1.

2. Mathematical formulation based on a development of Jeffery–Hamel problem

Let us to consider cylindrical polar coordinates (r, θ, z) , which the steady laminar 2D flow of an incompressible hybrid nanofluid from a sink or source at duct walls lie in planes and intersect in z -axis under the influence of velocity slip, viscous dissipation and temperature jump. The problem diagram is shown in Figure 1. Here, we suppose that $v = 0$; there are no changes with respect to z direction; therefore the motion is completely in r direction and merely depends on r and θ (Rana *et al.*, 2019). According to the single-phase Tiwari and Das (Sheikholeslami and Shamlooei, 2017) model, both base liquid and nanoparticles are in thermal equilibrium and also there is no slip among them. It is also assumed that, at first, titanium dioxide (Ti_2O) and then Silver (Ag) are diffused inward the base liquid. The hybrid nanofluid is assumed to be single phase, and nanoparticles are dispersed homogeneously in the base fluid. Therefore, the stability issue of the hybrid nanofluid in terms of aggregation and agglomeration will be ignored in the present work (Dinarvand *et al.*, 2022). Table 2 presents the properties of solid particles and blood.

Under above assumptions, our governing PDEs including mass, momentum and energy conservations can be presented as (Rana *et al.*, 2019; Tiwari and Das, 2007; Chandra Roy, 2020; Li *et al.*, 2018):

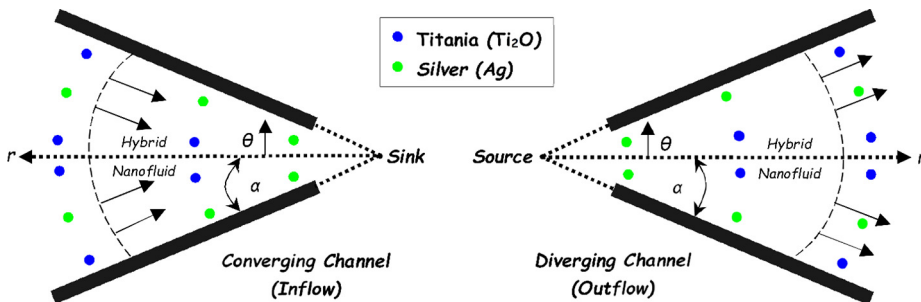


Figure 1. General diagram of converging/diverging duct flow

$$\frac{\rho_{hnf}}{r} \frac{\partial(r u(r, \theta))}{\partial r} = 0, \tag{1}$$

$$u(r, \theta) \frac{\partial u(r, \theta)}{\partial r} = \frac{-1}{\rho_{hnf}} \frac{\partial P}{\partial r} + \frac{\mu_{hnf}}{\rho_{hnf}} \left(\frac{\partial^2 u(r, \theta)}{\partial r^2} + \frac{1}{r} \frac{\partial u(r, \theta)}{\partial r} + \frac{1}{r^2} \frac{\partial^2 u(r, \theta)}{\partial \theta^2} - \frac{u(r, \theta)}{r^2} \right), \tag{2}$$

$$\frac{-1}{\rho_{hnf}} \frac{\partial P}{\partial \theta} + \frac{2\mu_{hnf}}{r\rho_{hnf}} \frac{\partial u(r, \theta)}{\partial r} = 0, \tag{3}$$

$$u(r, \theta) \frac{\partial T}{\partial r} = \frac{k_{hnf}}{(\rho C_p)_{hnf}} \left(\frac{\partial^2 T}{\partial r^2} + \frac{1}{r} \frac{\partial T}{\partial r} + \frac{1}{r^2} \frac{\partial^2 T}{\partial \theta^2} \right) + \frac{\mu_{hnf}}{(\rho C_p)_{hnf}} \left(4 \left(\frac{\partial u(r, \theta)}{\partial r} \right)^2 + \frac{1}{r^2} \left(\frac{\partial u(r, \theta)}{\partial \theta} \right)^2 \right), \tag{4}$$

Subject to the dimensional boundary conditions (Rana *et al.*, 2019; Tiwari and Das, 2007; Chandra Roy, 2020; Li *et al.*, 2018):

$$\begin{aligned} \frac{\partial u}{\partial \theta} = 0, \quad \frac{\partial T}{\partial \theta} = 0, \quad u = U, \quad \text{at } \theta = 0, \\ u = -N_1 v_{hnf} \frac{\partial u}{\partial \theta}, \quad T = \frac{T_w}{r^2} - D_1 \frac{\partial T}{\partial \theta} \quad \text{at } \theta = \alpha. \end{aligned} \tag{5}$$

where U is an arbitrary velocity, N_1 is the dimensional velocity slip coefficient, D_1 is the dimensional temperature jump parameter, α is the semiangle between the two inclined walls and P is the pressure field. Further, the effective properties of hybrid nanofluid containing dynamic viscosity (μ), thermal conductivity (K), volumetric heat capacity (ρC_p) and density (ρ), as shown in Table 3. In Table 3, ϕ is the total volume fraction and n is the shape factor ($n = 3/\psi$), where ψ is the sphericity (Figure 2).

Table 2.
Properties of pure blood and the applied nanosolid particles (Turkyilmazoglu, 2014)

Property	Pure blood	Titanium dioxide (Ti ₂ O)	Silver (Ag)
ρ	1,063	4,250	10,500
C_p	3,594	686.2	235
k	0.492	8.954	429

Table 3.
Properties of hybrid nanofluid (effective models applied in the present work) (Dinarvand and Rostami, 2019; Dinarvand *et al.*, 2019; Dinarvand *et al.*, 2022)

Properties	Formulation
Density	$\rho_{hnf} = (1 - \phi)\rho_f + \phi\rho_s$
Heat capacitance	$(\rho c_p)_{hnf} = (1 - \phi)(\rho c_p)_f + \phi(\rho c_p)_s$
Dynamic viscosity	$\mu_{hnf} = \frac{\mu_f}{(1 - \phi)^{2.5}}$
Thermal conductivity	$\frac{k_{hnf}}{k_{nf}} = \frac{k_{s2} + (n_2 - 1)k_{nf} - (n_2 - 1)\phi_2(k_{nf} - k_{s2})}{k_{s2} + (n_2 - 1)k_{nf} + \phi_2(k_{nf} - k_{s2})}$
	$\frac{k_{nf}}{k_f} = \frac{k_{s1} + (n_1 - 1)k_f - (n_1 - 1)\phi_1(k_f - k_{s1})}{k_{s1} + (n_1 - 1)k_f + \phi_1(k_f - k_{s1})}$

From work of Dinarvand and Nademi Rostami (Dinarvand and Rostami, 2019), the first nanoparticle volume fraction (ϕ_1), the second nanoparticle volume fraction (ϕ_2) and the equivalent volume fraction (ϕ), the equivalent specific heat $[(C_p)_s]$ and the equivalent density (ρ_s) are introduced in Table 4.

According to Rana *et al.* (2019) and Tiwari and Das (2007), we can present the similarity variables as follows:

$$\eta = \frac{\theta}{\alpha}, \quad f(\theta) = r u(r, \theta), \quad \Theta(\eta) = r^2 \frac{T}{T_w}, \quad (6)$$

Substituting equation (12) into PDEs (1)–(4), the below ODEs are obtained:

$$f''' + 2\alpha Re \left(1 - \frac{\frac{m_1 + m_2}{\rho_1} + \frac{m_2}{\rho_2} + \frac{m_f}{\rho_f}}{\frac{m_1 + m_2}{\rho_1} + \frac{m_2}{\rho_2} + \frac{m_f}{\rho_f}} \right)^{2.5} \left(1 - \frac{\frac{m_1 + m_2}{\rho_1} + \frac{m_2}{\rho_2} + \frac{m_f}{\rho_f}}{\frac{m_1 + m_2}{\rho_1} + \frac{m_2}{\rho_2} + \frac{m_f}{\rho_f}} + \frac{\frac{m_1 + m_2}{\rho_1} + \frac{m_2}{\rho_2}}{\frac{m_1 + m_2}{\rho_1} + \frac{m_2}{\rho_2} + \frac{m_f}{\rho_f}} \frac{\rho_s}{\rho_f} \right) [f f'] + 4\alpha^2 f' = 0, \quad (7)$$

$$\frac{k_{inf}}{k_f} (\Theta + 4\alpha^2 \Theta) + 2\alpha^2 Pr \left(1 - \frac{\frac{m_1 + m_2}{\rho_1} + \frac{m_2}{\rho_2} + \frac{m_f}{\rho_f}}{\frac{m_1 + m_2}{\rho_1} + \frac{m_2}{\rho_2} + \frac{m_f}{\rho_f}} + \frac{\frac{m_1 + m_2}{\rho_1} + \frac{m_2}{\rho_2}}{\frac{m_1 + m_2}{\rho_1} + \frac{m_2}{\rho_2} + \frac{m_f}{\rho_f}} \frac{(\rho C_p)_s}{(\rho C_p)_f} \right) (f \cdot \Theta) + \frac{Pr Ec}{Re} (4\alpha^2 f^2 + f'^2) = 0, \quad (8)$$

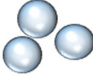




Nanoparticle shapes	Sphere	Brick	Cylinder	Platelet	Disk
Shape structure					
ψ	1	0.81	0.62	0.52	0.36
n	3	3.7	4.8	5.7	8.3

Figure 2. Shape factor and sphericity (Timofeeva *et al.*, 2009; Sheikholeslami and Shamlooei, 2017)

Title	Mathematical relations
Equivalent density	$\rho_s = \frac{(\rho_1 \times m_1) + (\rho_2 \times m_2)}{m_1 + m_2}$
Equivalent specific heat of nanoparticles at constant pressure	$(C_p)_s = \frac{((C_p)_1 \times m_1) + ((C_p)_2 \times m_2)}{m_1 + m_2}$
Solid volume fraction of first nanoparticle	$\phi_1 = \frac{\frac{m_1}{\rho_1}}{\frac{m_1}{\rho_1} + \frac{m_2}{\rho_2} + \frac{m_f}{\rho_f}}$
Solid volume fraction of second nanoparticle	$\phi_2 = \frac{\frac{m_2}{\rho_2}}{\frac{m_1}{\rho_1} + \frac{m_2}{\rho_2} + \frac{m_f}{\rho_f}}$
Equivalent volume fraction of nanoparticles	$\phi = \phi_1 + \phi_2 = \frac{\frac{\rho_s}{m_1 + m_2} + \frac{m_f}{\rho_f}}{\rho_s}$

Table 4. Definitions based on mass-based model (Dinarvand and Rostami, 2019; Dinarvand *et al.*, 2019; Dinarvand *et al.*, 2022)

Similarly, substituting equation (12) into equation (5) will give:

$$f(0) = 1, \quad f'(0) = 0, \quad \Theta'(0) = 0, \quad (9)$$

$$f(1) = \frac{-af'(1)}{\left(1 - \frac{m_1 + m_2}{\rho_1 + \rho_2}\right)^{2.5} \left(1 - \frac{m_1 + m_2}{\rho_1 + \rho_2 + \frac{m_f}{\rho_f}} + \frac{m_1 + m_2}{\rho_1 + \rho_2 + \frac{m_f}{\rho_f}} \frac{\rho_s}{\rho_f}\right)}, \quad \Theta(1) = 1 - b\Theta'(1). \quad (10)$$

In which, a and b are the velocity slip and the temperature jump parameter, respectively. The governing parameters of the present problem are defined as (Rana *et al.*, 2019; Tiwari and Das, 2007):

$$a = \frac{N_1 v_f}{\alpha}, \quad b = \frac{D_1}{\alpha}, \quad Ec = \frac{U^2}{T_w(C_P)_f}, \quad Re = \frac{U r \alpha}{v_f}, \quad Pr = \frac{v_f(\rho C_P)_f}{k_f}. \quad (11)$$

The quantities of engineering interest can be defined as (Rana *et al.*, 2019; Tiwari and Das, 2007):

$$C_f = \frac{\tau_w}{\rho_f U^2}, \quad \tau_w = \frac{\mu_{hnf}}{r} \left(\frac{\partial u}{\partial \theta}\right)_{\theta=\alpha}, \quad (12)$$

$$Nu = \frac{r q_w}{k_f(T_w)}, \quad q_w = -k_{hnf} \left(\frac{1}{r} \frac{\partial T}{\partial \theta}\right)_{\theta=\alpha},$$

where q_w and τ_w are the surface heat flux and the surface shear stress, respectively. Substituting equation (6) into equation (12), gives below relations:

$$C_f Re = \frac{1}{r^2} \left(1 - \frac{m_1 + m_2}{\rho_1 + \rho_2 + \frac{m_f}{\rho_f}}\right)^{-2.5} f'(1), \quad Nu = \frac{-r k_{hnf}}{\alpha k_f} \Theta'(1), \quad (13)$$

3. Results and discussion

First, Table 5 has been prepared to present the values of the emerging parameters applied in this study. This helps better realization of results for readers.

Table 5.
Values of the
emerging parameters
in this study

Governing parameter	Symbol	Used values
First nanoparticle mass	m_1	{0,10}
Second nanoparticle mass	m_2	{0,15,30}
Base fluid mass	m_f	{100}
Eckert number	Ec	{0.1,0.2,0.3}
Reynolds number	Re	{50,80,150,250}
Open angle	A	{ $\pm 3^\circ$, $\pm 5^\circ$, $\pm 7^\circ$ }
Shape factor	N	{3.3,7,4.8,5.7,8.3}
Velocity slip and the temperature jump parameter	a and b	{0,0.2,0.5}
Prandtl number	Pr	{21,23,25}

The governing equations (1)–(4) are transformed to the set of coupled nonlinear ODEs (7)–(8) using similarity method, which are numerically solved for different values of the emerging parameters. The solution procedure is based on RKF technique. Here, $\Delta\eta = 0.001$ is step size and the criteria of convergence is 10^{-6} in the program. In operation, $\eta = \infty$ must be replaced by an approximation $\eta = \eta_{\max}$, where η_{\max} is optional as long as it is chosen great enough so that the solution demonstrates small further change for η greater than η_{\max} .

To evaluate the accuracy of the present results, the validity of the computational code has been explored for some special cases. Table 6 shows the values of $-f'''(0)$ for various values of open angle (α) and Reynolds number (Re), when $m_1 = m_2 = 0$ gr, $m_f = 100$ gr, $a = 0$. In Table 6, a comparison is performed with already published results of Turkyilmazoglu (Turkyilmazoglu, 2014; Khan and Ahmed, 2017; Mohamed *et al.*, 2018) and Berrehal and Sowmya (Berrehal and Sowmya, 2021) that demonstrates a favorable agreement with the present work.

Before the presentation of the results, it is important to describe the importance of the selected nanoparticles. Many studies have demonstrated the usefulness of these nanoparticles (titania and silver) for diagnosis, tumor targeting and therapy. Moreover, the high doses of therapeutic agents can be delivered by particles with nanodimensions within tumor cells without spattering other cells. Besides, the nanoparticles of titania and silver have removed many common chemotherapy deficiencies for example drug resistance, nonspecific distribution and unwanted side effects.

Here, an analysis of the thermal and hydrodynamic behavior for diverging/converging channel flow based on different controlling parameters will be performed and discussed. Temperature and velocity for different values of Re for both cases of the diverging and

α	Re	Turkyilmazoglu (2014)	Khan <i>et al.</i> (2021)	Mohamed <i>et al.</i> (2018)	Berrehal and Sowmya (2021)	Present work
+5	20	2.52719	2.52719	2.52719	2.52719	2.52719
	60	3.94214	3.94214	3.94214	3.94214	3.94214
	100	5.86916	5.86916	5.86916	5.86916	5.86916
-5	30	1.41369	1.41369	1.41369	1.41369	1.41369
	70	0.89347	0.89347	0.89347	0.89347	0.89347
	100	0.64017	0.64017	0.64017	0.64017	0.64017

Table 6. Comparison of $-f'''(0)$ for various values of open angle (α) and Reynolds number (Re) when $m_1 = m_2 = 0$ gr, $m_f = 100$ gr, $a = 0$

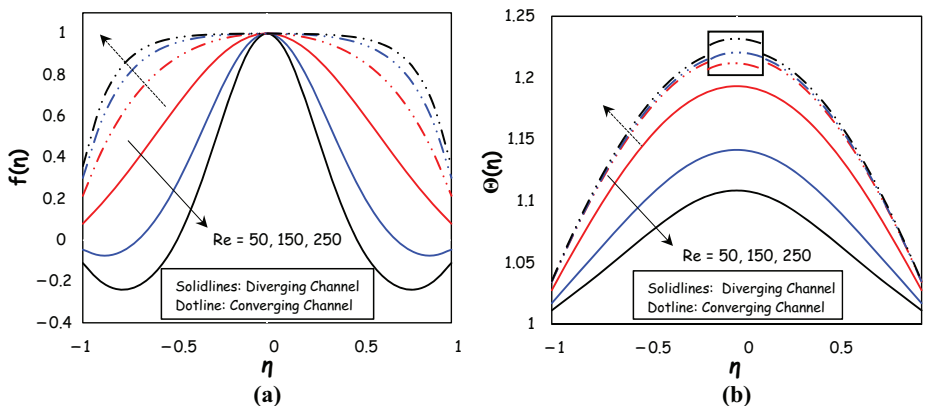


Figure 3. Velocity and temperature for various values of Reynolds number (Re) for diverging channel ($\alpha = +5$) and converging channel ($\alpha = -5$) when $m_1 = m_2 = 10$ gr, $m_f = 100$ gr, $n_1 = n_2 = 3$, $a = b = 0.1$, $Ec = 0.1$ and $Pr = 21$

converging channels have been plotted in Figure 3. The velocity reduces with Re for the diverging channel, while an augmentation in velocity would be observed for the converging case. Temperature also has a similar manner with the change in Re for both cases. Although for the cases of converging channel, the effect of Re on the temperature distribution is too gentle.

Figure 4 has been plotted to demonstrate the effect of various values of open angle α on the velocity profile and temperature distribution for both diverging and converging channels. A reduction is seen with open angle for the diverging channel, and there is an opposite trend for the converging channel. The effect of open angle on temperature is subtractive for both cases of diverging and converging channels.

Temperature distribution and velocity profile for various values of second nanoparticle mass m_2 for both cases of the diverging and converging channels are shown in Figure 5. For the diverging channel, a decrease in the velocity of hybrid nanofluid is appeared with the enhancement in m_2 (second nanoparticle mass), while an opposite manner is observed for the converging case. Moreover, the second nanoparticle mass compresses the temperature distribution for both types of channels. Thus, the heat transfer features of the working fluid flow will be influenced by the temperature distribution changes.

Figure 4. Velocity and temperature for various values of open angle (α) for diverging and converging channels when $Re = 80, m_1 = m_2 = 10$ gr, $m_f = 100$ gr, $n_1 = n_2 = 3, a = b = 0.1, Ec = 0.1$ and $Pr = 21$

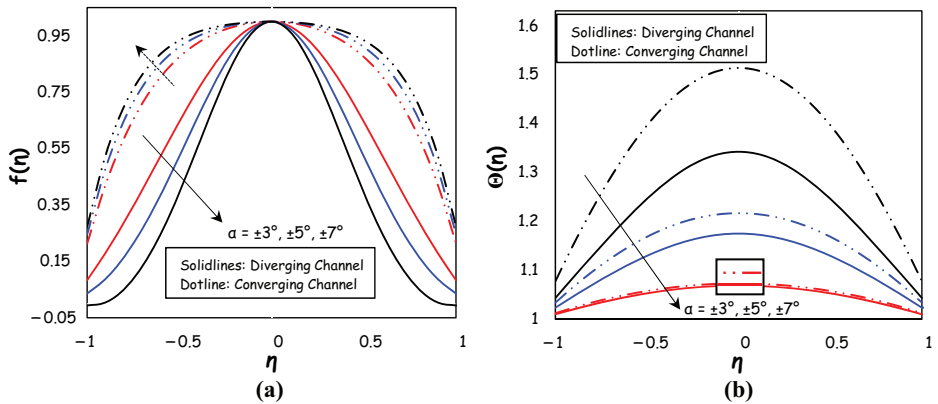


Figure 5. Velocity and temperature for various values of the second nanoparticle mass (m_2), for diverging channel ($\alpha = +5$) and converging channel ($\alpha = -5$) when $Re = 80, m_1 = 10$ gr, $m_f = 100$ gr, $n_1 = n_2 = 3, a = b = 0.1, Ec = 0.1$ and $Pr = 21$

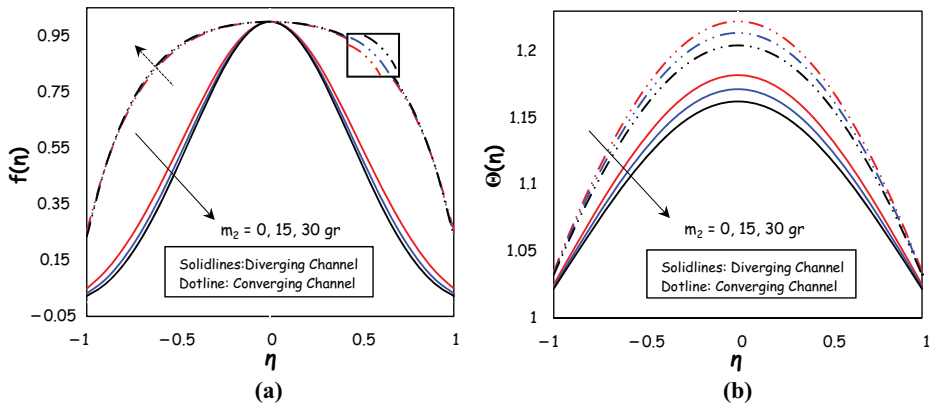


Figure 6 illustrates the velocity profile and temperature distribution with different values of the velocity slip parameter for diverging and converging channels. The velocity increases with the slip parameter for both the cases, although this parameter has a more great influence on the velocity of the converging channel. Besides, a smooth and gentle enhancement of temperature in the channel can be observed with the slip parameter.

Temperature distribution for various values of temperature jump parameter (b) and Prandtl number (Pr) for the diverging channel ($\alpha = +5$) and converging channel ($\alpha = -5$) has been plotted in Figure 7. This figure demonstrates that hybrid nanofluid temperature augments strongly with the jump parameter. About the effect of the Pr on the temperature, it is clear that with the increase in Pr , temperature also enhances for both cases of diverging and converging channels.

The effect of the Eckert number (Ec) and nanoparticle shape factor n on temperature distribution for the diverging channel ($\alpha = +5$) and converging channel ($\alpha = -5$) have been shown in Figure 8. The temperature decreases with the Ec , while the nanoparticle shape factor enhances the hybrid nanofluid temperature for both types of channels.

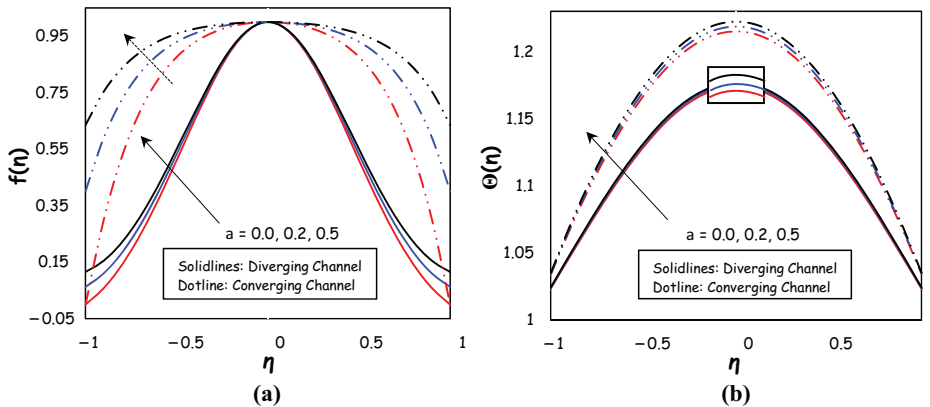


Figure 6. Velocity and temperature for various values of velocity slip parameter (a) for diverging channel ($\alpha = +5$) and converging channel ($\alpha = -5$) when $Re = 80$, $m_1 = m_2 = 10$ gr, $m_f = 100$ gr, $n_1 = n_2 = 3$, $b = 0.1$, $Ec = 0.1$ and $Pr = 21$

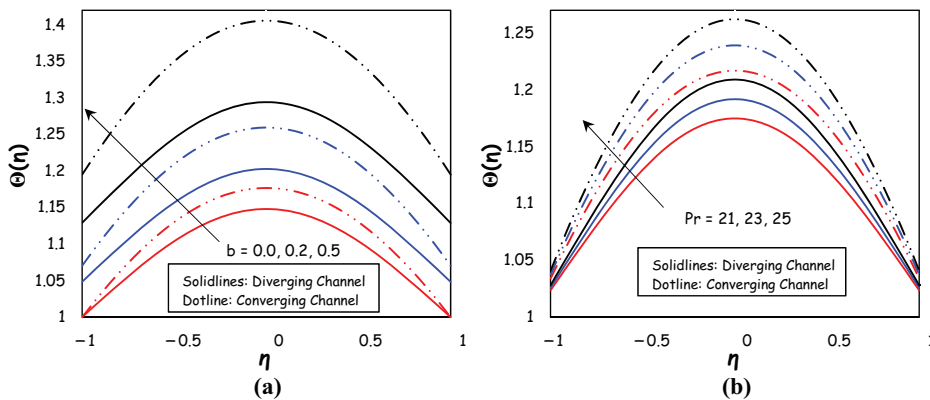


Figure 7. Temperature distribution for various values of temperature jump parameter (b) and Prandtl number (Pr) for diverging channel ($\alpha = +5$) and converging channel ($\alpha = -5$) when $Re = 80$, $m_1 = m_2 = 10$ gr, $m_f = 100$ gr, $n_1 = n_2 = 3$, $a = b = 0.1$, $Ec = 0.1$ and $Pr = 21$

Figure 9 (a) and (b) presents to show the skin friction coefficient and the Nusselt number for different states such as the regular fluid (pure blood), mononanofluids (titanium dioxide/water and silver/water) and hybrid nanofluids (titanium dioxide–silver/water) considering various values of titanium dioxide and silver nanoparticle masses. These figures show the results for both cases of diverging and converging channels. Table 7 illustrates a list of abbreviations for various cases of working fluids that are applied in this research. The Nusselt number and skin friction increase with the enhancement of both nanoparticles (titanium dioxide and silver). This occurs because of the augmentation of equivalent thermal conductivity that has an enhancing effect on the heat transfer characteristics of the hybrid nanofluid. It is worth mentioning the Nusselt number is low when titania is dispersed within the base liquid (blood) while it strongly enhances by adding the second nanoparticle (silver) in cases of NF3 and NF4. Obviously, the thermal conductivity of silver is higher than titania which causes this result. To compare thermal conductivities and more analysis, readers can refer to Table 2.

Figure 8. Temperature distribution for various values of Eckert number (Ec) and nanoparticle shape factor (n) for diverging channel ($\alpha = +5$) and converging channel ($\alpha = -5$) when $Re = 80$, $m_1 = m_2 = 10$ gr, $m_f = 100$ gr, $n_1 = n_2 = 3$, $a = b = 0.1$, $Ec = 0.1$ and $Pr = 21$

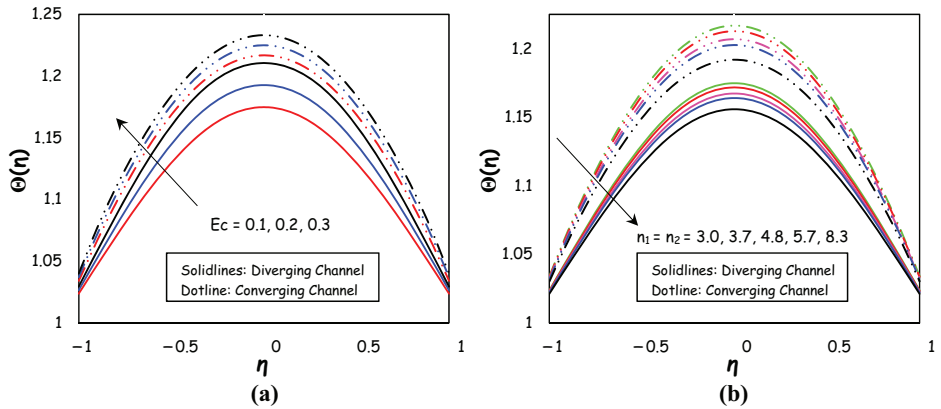
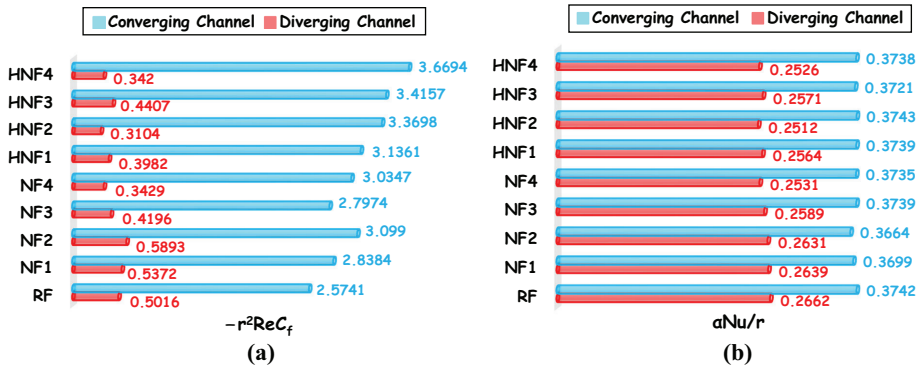


Figure 9. Skin friction coefficient $-r^2ReC_f$ and Nusselt number aNu/r for various types of working fluid indexed in Table 7, for diverging channel ($+ \alpha$) and converging channel ($- \alpha$) when $Re = 80$, $m_1 = m_2 = 10$ gr, $m_f = 100$ gr, $n_1 = n_2 = 3$, $a = b = 0.1$, $Ec = 0.1$ and $Pr = 21$



The nanoparticle shape is a significant factor in the behavior of hybrid nanofluids in view of flow and heat transfer. In fact, the shape of a particle affects its motion and kind of dispersion in a base liquid. It is obvious that the nonspherical nanoparticles move differently from spherical nanoparticles in rotational and translational forms. When we have nonspherical particles, the opposing forces from the side of the base fluid are more than when there are spherical particles. This issue demonstrates that the rheology of a hybrid nanofluid is strongly dependent on the shape of particles. Finally, the present concept is also significant and effective to the heat transfer features of a solid-liquid suspension. Figure 10(a) and (b) presents the influence of the nanoparticle shape on the Nusselt number for both cases of diverging and converging channels.

The results of $-f'(1)$ for various values of open angle (α), Re, velocity slip parameter (a), the second nanoparticle mass (m_2), for both diverging channel ($+\alpha$) and converging channel ($-\alpha$) have reported in Table 8. Here, one can analyze the effect of the emerging parameters of problem on heat and fluid flow characteristics. Besides, Table 9 depicts the results of $-\theta'(1)$ for various values of open angle (α), Re, the second nanoparticle mass (m_2), temperature jump parameter (b), Ec and nanoparticle shape factor (n), for both diverging channel ($+\alpha$) and converging channel ($-\alpha$).

Finally, the contour plots of streamlines for both cases of diverging ($\alpha = -5$) and diverging channel ($\alpha = +5$) have been presented in Figure 11(a) and (b), when $Re = 80$, $m_1 = m_2 = 0$ gr, $m_f = 100$ gr, $a = b = 0$, $Ec = 0.1$ and $Pr = 21$. Besides, Figure 12(a) and (b) shows the contour plots of isotherms for the same conditions as Figure 11(a) and (b).

Types	Description	m_1 (gr)	m_2 (gr)
RF	Regular fluid	0	0
NF1	Nanofluid (type 1)	15	0
NF2	Nanofluid (type 2)	30	0
NF3	Nanofluid (type 3)	0	15
NF4	Nanofluid (type 4)	0	30
HNF1	Hybrid nanofluid (type 1)	15	15
HNF2	Hybrid nanofluid (type 2)	15	30
HNF3	Hybrid nanofluid (type 3)	30	15
HNF4	Hybrid nanofluid (type 4)	30	30

Table 7. Index for Figure 8

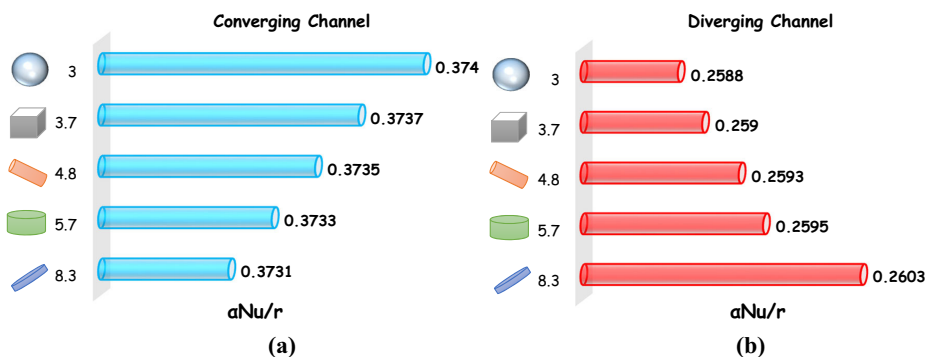


Figure 10. Nusselt number $\alpha Nu/r$ for various values of nanoparticle shape factor (n), for diverging channel ($\alpha = +5$) and converging channel ($\alpha = -5$) when $Re = 80$, $m_1 = m_2 = 10$ gr, $m_f = 100$ gr, $a = b = 0.1$, $Ec = 0.1$ and $Pr = 21$

4. Conclusions

Here, the viscous flow and heat transfer of a hybrid nanofluid passing through a converging/diverging channel has been explored. The nanoparticles are the titanium dioxide (Ti₂O) and silver (Ag) in different shapes of sphere, brick, cylinder, platelet and disk dispersed in the blood as base fluid. This new mass-based method is a single-phase hybrid nanofluid approach that the inputs are masses of nanoparticles and base liquid. The partial differential equations of the mass, momentum and energy after transforming to a set of ODEs are solved by the Runge–Kutta–Fehlberg procedure and shooting method. The validation is performed by comparing the present results with the already published achievements. The main conclusions from this study are as follows:

Table 8.

Results of $-f'(1)$ for various values of open angle (α), Reynolds number (Re), velocity slip parameter (a), the second nanoparticle mass (m_2), for diverging channel ($+\alpha$) and converging channel ($-\alpha$) when $m_1 = 10$ gr, $m_f = 100$ gr, and $Pr = 21$

Re	m_2	a	A	Diverging Channel	α	Converging Channel
30	10	0.1	5°	1.210945	-5°	2.118015
60				0.712690		2.489957
90				0.239957		2.809880
50	0			0.937137		2.280412
	15			0.857047		2.403268
	30			0.804271		2.477243
	10	0		1.019516		2.915150
		0.2		0.776065		1.981085
		0.4		0.635751		1.475597
		0.1	2°	1.377933	-2°	1.984100
			4°	1.046562	-4°	2.249254
			6°	0.710637	-6°	2.488844

Table 9.

Results of $-\theta'(1)$ for various values of open angle (α), Reynolds number (Re), the second nanoparticle mass (m_2), temperature jump parameter (b), eckert number (Ec) and nanoparticle shape factor (n), for diverging channel ($+\alpha$) and converging channel ($-\alpha$), when $m_1 = 10$ gr, $m_f = 100$ gr, $a = 0.1$ and $Pr = 21$

Re	m_2	b	Ec	n	α	Diverging Channel	α	Converging Channel
30	10	0.1	0.1	3	5°	0.319297	-5°	0.363638
60						0.261628		0.343242
90						0.225464		0.341937
50	0					0.287845		0.353341
	15					0.271250		0.341432
	30					0.256788		0.327948
	10	0				0.270211		0.335845
		0.2				0.283242		0.356725
		0.4				0.297593		0.380373
		0.1	0.1			0.276573		0.345970
			0.2			0.317703		0.390457
			0.3			0.358833		0.434944
			0.1	3.7		0.271707		0.339651
				4.8		0.264745		0.330615
				5.7		0.259576		0.323913
				8.3		0.246723		0.307260
				3	2°	0.073622	-2°	0.079340
					4°	0.187521	-4°	0.222143
					6°	0.391212	-6°	0.520578

- The velocity near the walls reduces with Re , m_2 and α for the diverging channel because of the decrease of the pressure gradient, while an augmentation in velocity would be observed for the converging case.
- The velocity increases with the slip parameter for both diverging/converging channel.
- Backflow regimes forms in the divergent channel for high Re , m_2 and α values and low value of.
- Thickness of a thermal boundary layer reduces with α , m_2 and n_2 and enhances with a , b , Pr and Ec for both divergent/converging channels.
- Thickness of thermal boundary layer reduces with Re for divergent channels and increases in converging cases.

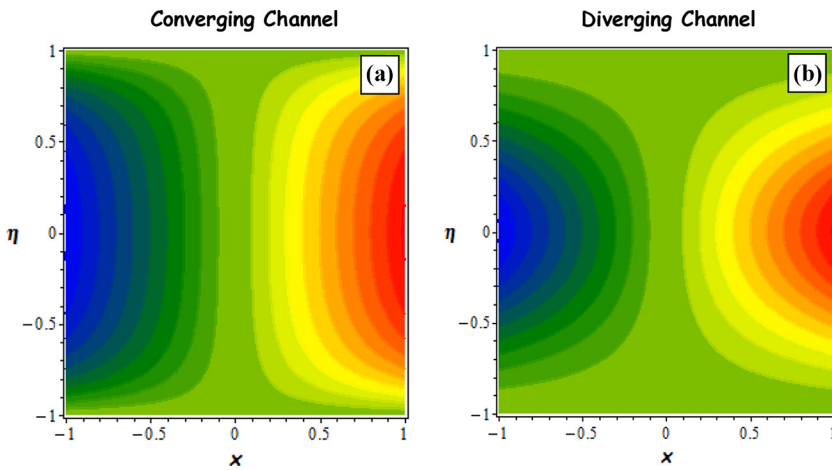


Figure 11. Contour plots of streamlines for converging channel ($\alpha = -5$) and diverging channel ($\alpha = +5$) when $Re = 80$, $m_1 = m_2 = 0$ gr, $m_f = 100$ gr, $a = b = 0$, $Ec = 0.1$ and $Pr = 21$

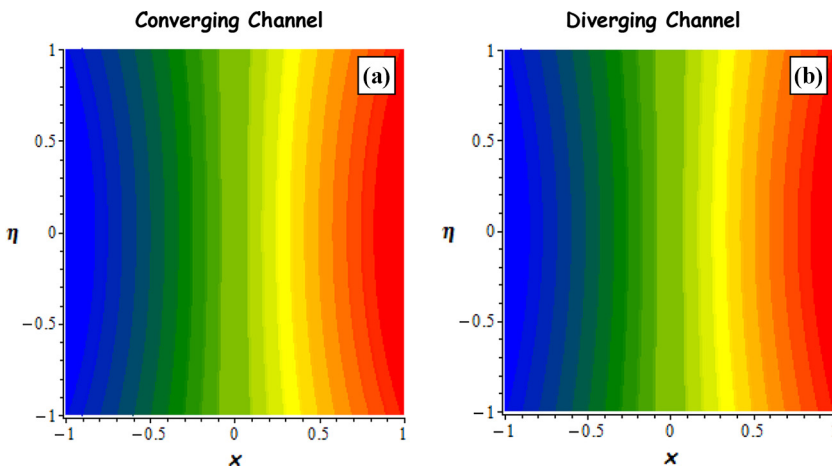


Figure 12. Contour plots of isotherms for converging channel ($\alpha = -5$) and diverging channel ($\alpha = +5$) when $Re = 80$, $m_1 = m_2 = 0$ gr, $m_f = 100$ gr, $a = b = 0$, $Ec = 0.1$ and $Pr = 21$

- The Nusselt number and skin friction coefficient augments with the enhancement in first (titanium dioxide) and second (silver) nanoparticle masses for the converging/diverging channel.
- Finally, the mass-based model with its great benefits such as simplicity of usage and the computation of thermophysical properties of hybrid nanofluid with help of both nanoparticles and base fluid masses can be excellently applied to different problems with high confidence.

References

- Afshari, F., Tuncer, A.D., Sözen, A., Variyenli, H.I., Khanlari, A. and Gürbüz, E.Y. (2021), "A comprehensive survey on utilization of hybrid nanofluid in plate heat exchanger with various number of plates", *International Journal of Numerical Methods for Heat and Fluid Flow*, Vol. 32 No. 1, pp. 241-264.
- Agrawal, P., Dadhech, P.K., Jat, R.N. and Baleanu, S.D. (2021), "Radiative MHD hybrid-nanofluids flow over a permeable stretching surface with heat source/sink embedded in porous medium", *International Journal of Numerical Methods for Heat and Fluid Flow*, Vol. 31 No. 8, pp. 2818-2840.
- Ahmed, J., Shahzad, A., Farooq, A., Kamran, M., Ud-Din Khan, S. and Ud-Din Khan, S. (2021), "Thermal analysis in swirling flow of titanium dioxide–aluminum oxide water hybrid nanofluid over a rotating cylinder", *Journal of Thermal Analysis and Calorimetry*, Vol. 144 No. 6, pp. 2175-2185.
- Ahmed, N., Abbasi, A., Khan, U. and Mohyud-Din, S.T. (2018), "Thermal radiation effects on flow of jeffery fluid in converging and diverging stretchable channels", *Neural Computing and Applications*, Vol. 30 No. 8, pp. 2371-2379.
- Berrehal, H. and Sowmya, G. (2021), "Heat transfer analysis of nanofluid flow in a channel with non-parallel walls", *Journal of Mechanical Science and Technology*, Vol. 35 No. 1, pp. 171-177.
- Berrehal, H. and Makinde, O.D. (2021), "Heat transfer analysis of CNTs-water nanofluid flow between nonparallel plates: approximate solutions", *Heat Transfer*, Vol. 50 No. 5, pp. 4978-4992.
- Berrehal, H., Dinarvand, S. and Khan, I. (2022), "Mass-based hybrid nanofluid model for entropy generation analysis of flow upon a convectively-warmed moving wedge", *Chinese Journal of Physics*, Vol. 77, pp. 2603-2616.
- Chandra Roy, N. (2020), "Mathematical approach of demarcation of dual solutions for a flow", *Chinese Journal of Physics*, Vol. 68, pp. 514-532.
- Das, P.K. (2017), "A review based on the effect and mechanism of thermal conductivity of normal nanofluids and hybrid nanofluids", *Journal of Molecular Liquids*, Vol. 240, pp. 420-446.
- Dinarvand, S. and Rostami, M.N. (2019), "An innovative mass-based model of aqueous zinc oxide–gold hybrid nanofluid for von Karman's swirling flow", *Journal of Thermal Analysis and Calorimetry*, Vol. 138 No. 1, pp. 845-855.
- Dinarvand, S., Nademi Rostami, M. and Pop, I. (2019), "A novel hybridity model for TiO₂-CuO/water hybrid nanofluid flow over a static/moving wedge or corner", *Scientific Reports*, Vol. 9 No. 1, p. 16290.
- Dinarvand, S., Mousavi, S.M., Yousefi, M. and Rostami, M.N. (2022), "MHD flow of MgO-Ag/water hybrid nanofluid past a moving slim needle considering dual solutions: an applicable model for hot-wire anemometer analysis", *International Journal of Numerical Methods for Heat and Fluid Flow*, Vol. 32 No. 2, pp. 488-510.
- Jaballah, R.B., HamidaSaleh, M.B.B.J. and Almeshaal, M.A. (2019), "Enhancement of the performance of bubble absorber using hybrid nanofluid as a cooled absorption system", *International Journal of Numerical Methods for Heat and Fluid Flow*, Vol. 29 No. 10, pp. 3857-3871.
- Jana, S., Salehi-Khojin, A. and Zhong, W.-H. (2007), "Enhancement of fluid thermal conductivity by the addition of single and hybrid nano-additives", *Thermochim Acta*, Vol. 462 Nos 1/2, pp. 45-55.

- Khan, U., Zaib, A., Bakar, S.A. and Ishak, A. (2021), “Stagnation-point flow of a hybrid nanofluid over a non-isothermal stretching/shrinking sheet with characteristics of inertial and microstructure”, *Case Studies in Thermal Engineering*, Vol. 26, p. 101150.
- Khan, U.N. and Ahmed, S.T. (2017), “Mohyud-Din, heat transfer effects on carbon nanotubes suspended nanofluid flow in a channel with non-parallel walls under the effect of velocity slip boundary condition: a numerical study”, *Neural Computing and Applications*, Vol. 28 No. 1, pp. 37-46.
- Li, Y., Shahsavari, A. and Talebizadehsardari, P. (2021), “Thermal conductivity of ethylene glycol-based nanofluid containing SiO₂ nanoadditives: experimental data and modeling through curve fitting”, *Journal of Thermal Analysis and Calorimetry*, Vol. 146 No. 3, pp. 1101-1109.
- Li, Z., Khan, I., Shafee, A., Tlili, I. and Asifa, T. (2018), “Energy transfer of jeffery–hamel nanofluid flow between non-parallel walls using maxwell–garnetts (MG) and brinkman models”, *Energy Reports*, Vol. 4, pp. 393-399.
- Mahian, O., Bellos, E., Markides, C.N., Taylor, R.A., Alagumalai, A., Yang, L., Qin, C., Lee, B.J., Ahmadi, G., Safaei, M.R. and Wongwises, S. (2021), “Recent advances in using nanofluids in renewable energy systems and the environmental implications of their uptake”, *Nano Energy*, Vol. 86, p. 106069.
- Menni, Y.A.G., Chamkha, N., Massarotti, H., Ameer, N., Kaid. and M., Bensafi. (2020), “Hydrodynamic and thermal analysis of water, ethylene glycol and water-ethylene glycol as base fluids dispersed by aluminum oxide nano-sized solid particles”, *International Journal of Numerical Methods for Heat and Fluid Flow*, Vol. 30 No. 9, pp. 4349-4386.
- Mohamed, K., Rafik, S.M., Rabah, B.O., Rashidi, M.M. and Ammar, H.A. (2018), “Heat transfer in hydro-magnetic nano-fluid flow between non-parallel plates using DTM”, *Journal of Applied and Computational Mechanics*, Vol. 4 No. 4, pp. 352-364.
- Patel, N. and Meher, R. (2018), “Analytical investigation of Jeffery-Hemal flow with magnetic field by differential transform method”, *The International Journal of Applied Mathematics and Mechanics*, Vol. 6, pp. 1-9.
- Rana, P., Shukla, N., Gupta, Y. and Pop, I. (2019), “Analytical prediction of multiple solutions for MHD jeffery–hamel flow and heat transfer utilizing KKL nanofluid model”, *Physics Letters A*, Vol. 383 Nos 2/3, pp. 176-185.
- Sheikholeslami, M. and Shamlooei, M. (2017), “Magnetic source influence on nanofluid flow in porous medium considering shape factor effect”, *Physics Letters A*, Vol. 381 No. 36, pp. 3071-3078.
- Sibanda, P., Motsa, S. and Makukula, Z. (2012), “A spectral-homotopy analysis method for heat transfer flow of a third-grade fluid between parallel plates”, *International Journal of Numerical Methods for Heat and Fluid Flow*, Vol. 22 No. 1, pp. 4-23.
- Sidik, N.A.C., Jamil, M.M., Japar, W. and Adamu, I.M. (2017), “A review on preparation methods, stability and applications of hybrid nanofluids”, *Renewable and Sustainable Energy Reviews*, Vol. 80, pp. 1112-1122.
- Sreedevi, P., Reddy, P.S. and Sheremet, M. (2020), “A comparative study of Al₂O₃ and TiO₂ nanofluid flow over a wedge with non-linear thermal radiation”, *International Journal of Numerical Methods for Heat and Fluid Flow*, Vol. 30 No. 3, pp. 1291-1317.
- Suresh, S., Venkitaraj, K.P., Selvakumar, P. and Chandrasekar, M. (2011), “Synthesis of Al₂O₃-Cu/water hybrid nanofluids using two step method and its thermophysical properties”, *Colloids and Surfaces A: Physicochemical and Engineering Aspects*, Vol. 388 Nos 1/3, pp. 41-48.
- Timofeeva, E.V., Routbort, J.L. and Singh, D. (2009), “Particle shape effects on thermophysical properties of alumina nanofluids”, *Journal of Applied Physics*, Vol. 106 No. 1, pp. 14304-14310.
- Tiwari, R.J. and Das, M.K. (2007), “Heat transfer augmentation in a two sided lid-driven differentially heated square cavity utilizing nanofluids”, *International Journal of Heat and Mass Transfer*, Vol. 50 Nos 9/10, pp. 2002-2018.

- Turkyilmazoglu, M. (2014), "Extending the traditional Jeffery-Hamel flow to stretchable convergent/divergent channels", *Computers and Fluids*, Vol. 100, pp. 196-203.
- Waini, I., Ishak, A. and Pop, I. (2021), "Hybrid nanofluid flow towards a stagnation point on an exponentially stretching/shrinking vertical sheet with buoyancy effects", *International Journal of Numerical Methods for Heat and Fluid Flow*, Vol. 31 No. 1, pp. 216-235.
- Waini, I., Ishak, A. and Pop, I. (2020), "Hiemenz flow over a shrinking sheet in a hybrid nanofluid", *Results in Physics*, Vol. 19, p. 103351.

Corresponding author

Saeed Dinarvand can be contacted at: sae.dinarvand@iauctb.ac.ir and saeed_dinarvand@yahoo.com